

SOME RESULTS ON A SEMICLASSICAL
DESCRIPTION OF A GRAVITATIONAL COLLAPSE*

J. WOSIEK

M. Smoluchowski Institute of Physics, Jagellonian University
Reymonta 4, 30-059 Kraków, Poland*(Received October 27, 2008)*

We review recent solutions of the classical equations of motion corresponding to the effective action of the linearized gravity. The action was derived by Amati, Ciafaloni and Veneziano to describe scattering of gravitating sources at very high energies. The solutions reveal a number of phenomena consistent with existence of a gravitational collapse in such a scattering.

PACS numbers: 04.70.Dy, 04.25.-g

1. Introduction

Even though the classic Schwarzschild metric is known for about a century, no analytical solution of Einstein equations, which actually describes the gravitational collapse and formation of a black hole, is available. On the other hand a significant progress in solving Einstein equations numerically has been achieved in the last decade and a number of precise numerical simulations of this phenomenon is available [1–3], see [4] for a recent review.

At the same time some analytical methods have been developed to describe a scattering of gravitating sources in the framework of the linearized gravity [5–7]. These lead to the derivation of the effective actions describing the, graviton mediated, high energy scattering of such sources [8–12].

In this paper I will report on the recent results obtained within the latter approach [13–15]. Interestingly a rich critical structure of the solutions is uncovered signaling possibly a collapse also in the high energy scattering.

* Presented at the XLVIII Cracow School of Theoretical Physics, “Aspects of Duality”, Zakopane, Poland, June 13–22, 2008.

1.1. Classical collapse and Choptuik scaling

To fix a notation and terminology we shall now briefly discuss numerical findings associated with the collapse [4]. One wants to solve the Einstein equations with a matter (described, *e.g.*, by a scalar field ϕ)

$$R^{\mu\nu} + \frac{1}{2}Rg^{\mu\nu} = 8\pi GT^{\mu\nu}, \quad \nabla_\mu \nabla^\mu \phi = 0 \quad (1)$$

and see which initial conditions

$$\phi(r, 0; p) \quad (2)$$

lead to a collapse. To this end a generic parameter (or a set of them) p is introduced which distinguishes the two situations:

1. $p < p^*$ no collapse — a system is said to be in a dispersive phase.
2. $p > p^*$ a collapse occurs — a system being in a black hole phase.

In 90's Choptuik has found that, if p is close to its critical value p^* , the solutions are locally selfsimilar [1]

$$\phi_*(sr, st) = \phi_*(r, t), \quad (3)$$

and, moreover, the mass of a black hole emerging for $p > p^*$ scales as a power

$$M(p) = c(p - p^*)^\gamma, \quad \gamma > 0, \quad (4)$$

with the “reduced” p . The exponent γ is universal depending only on a symmetry of a solution and on a type of a matter. These behaviours are in strong analogy with critical phenomena in statistical systems. In particular, two types of transitions were found. Namely, Type II transition with mass behaving as in (4), and Type I when a black hole with $M(p^*) \neq 0$ is created already at the transition point.

1.2. Linearized gravity, scattering and effective action

We now turn to the effective action approach. Derivation of the linearized gravity from the full Einstein–Hilbert action has a long history [12]. Some simplifications occur if one keeps only terms relevant for the high energy scattering, similarly to those which generate the multiregge asymptotics in QCD [9, 10]. Still the resulting actions are hardly manageable.

By summing eikonal diagrams augmented with a single emission from the exchanged line (the so called H diagram) Amati, Ciafaloni and Veneziano (ACV) have derived an effective action which is much simpler and is relevant

for the scattering in the so called transplanckian regime, *i.e.* $Gs \gg 1$, $s \gg t$ [8, 11, 13]. The ACV action reads

$$\begin{aligned} \mathcal{A} = & 2\pi Gs \int d^2\mathbf{x} \left[a_1(\mathbf{x})s_2(\mathbf{x}) + a_2(\mathbf{x})s_1(\mathbf{x}) - \frac{1}{2}\partial_i a_2 \partial_i a_1 \right. \\ & \left. + \frac{(\pi R)^2}{2}(-\partial_i \partial_i \phi)^2 + 2\phi \partial_i \partial_i \mathcal{H} \right], \\ \partial_i \partial_i \mathcal{H} = & -\partial_i \partial_i a_1 \partial_i \partial_i a_2 + \partial_i \partial_j a_1 \partial_i \partial_j a_2, \quad i = 1, 2, \end{aligned} \tag{5}$$

where $s_{1,2}(\mathbf{x})$ are transverse profiles of the left and right moving source, $a_{1,2}(\mathbf{x})$ describe exchanged gravitons which couple to $s_{2,1}$ respectively, and $\phi(\mathbf{x})$ is the field of a graviton emitted in the s -channel by three graviton vertex $\phi\mathcal{H}$. R is the Schwarzschild radius of the total CM energy, and $R_{1,2}$ are analogous, “running”, radii associated with the energies contained in the sources within a radius r from their respective centers.

$$R = 2G\sqrt{s}, \quad R_i(r) = 4GE_i(r), \quad r = |\mathbf{x}|, \quad R_i(\infty) = R, \tag{6}$$

$$\int d^2\mathbf{x}s(\mathbf{x}) = 1, \quad R_i(r) = R \int^r d^2\mathbf{x}s(\mathbf{x}). \tag{7}$$

Longitudinal degrees of freedom factorize giving rise to the overall factor of $Y = \log Gs$ *e.g.* in the production cross sections. The same action has been also derived in the momentum space

$$\begin{aligned} \mathcal{A} = & \frac{Gs}{2} \int \frac{d^2\mathbf{k}}{\mathbf{k}^2} \left[a_1(\mathbf{k})s_2(-\mathbf{k}) + a_2(\mathbf{k})s_1(-\mathbf{k}) \right. \\ & \left. - a_1(\mathbf{k})a_2(-\mathbf{k}) - \frac{(\pi R)^2}{2}[-h(\mathbf{k})h(-\mathbf{k}) - h(-\mathbf{k})\mathcal{H}(\mathbf{k})] \right]. \end{aligned} \tag{8}$$

In the next section we shall discuss classical equations of motion following from (5) and (8).

1.3. Effective equations of motion

Equations of motion in the configuration space are equivalent to a simple Coulomb problem with a repulsive, time dependent potential.

$$\ddot{\rho}(r) = \frac{1}{2} \frac{R_1(r)R_2(r)}{\rho^2(r)} \tag{9}$$

with $r^2 = \mathbf{x}^2$ playing a role of time: $\dot{} = d/dr^2$. The field ρ describes gravitons emitted in the s -channel.

$$\rho(r) = r^2(1 - 2\pi\dot{\phi}(r)), \tag{10}$$

We shall be seeking solutions of (9) with the following boundary conditions

$$\rho(0) = 0, \quad \rho(r) \sim r^2, \quad r \rightarrow \infty, \quad (11)$$

which eliminate singularity at $r = 0$ and guarantee smooth connection with the perturbative solution.

Corresponding equations in the momentum space read (assuming axial symmetry)

$$a_i(k^2) = s_i(k^2) + \frac{R^2}{8} \int \frac{dk_1^2 dk_2^2}{k_1^2 k_2^2} \sqrt{\lambda(k_1^2, k_2^2, k^2)} h(k_1^2) a_i(k_2^2),$$

$$h(k^2) = \frac{1}{4\pi^2} \int \frac{dk_1^2 dk_2^2}{k^2 k_1^2 k_2^2} \sqrt{\lambda(k_1^2, k_2^2, k^2)} a_1(k_1^2) a_2(k_2^2), \quad (12)$$

$$\lambda(k_1^2, k_2^2, k^2) = 2k_1^2 k_2^2 + 2k^2 k_2^2 + 2k_1^2 k^2 - k^4 - k_1^4 - k_2^4 \quad (13)$$

with all integrations running over the region allowed by the triangle relation between momenta of the exchanged and emitted gravitons.

2. Solutions and the onset of criticality

Before discussing how a collapse manifests itself in solutions of above equations, let us see how different scenarios may show up within the kinematics of high energy collisions. Classical scattering is described in terms of the CM energy \sqrt{s} (or R) and the impact parameter b . We have also allowed for the two more parameters, namely sizes of the sources $L_{1,2}$. When the impact parameter is large compared to the Schwarzschild radius R , the sources are deflected which causes some radiation hence multi graviton production. Nothing dramatic happens: we are in the dispersive phase. On the other hand for $b < R$, a lot of energy is concentrated below its Schwarzschild radius, therefore we expect that a collapse may occur — a black hole phase may develop.

2.1. Singularities in the momentum space solutions

These simple considerations suggest that the relevant parameter which could drive the transition is the dimensionless ratio R/b (or R/L)¹. Hence we expect that our solution of (9) and (12) may reveal some singular behaviour when R is increased. And indeed this is the case! The simplest way to see it, is to think of the iterative solution of the momentum space equations (12). The process is analogous to the generation of a geometric

¹ To simplify the discussion one could consider the head-on collisions. This eliminates one variable leaving R/L as the only essential parameter.

series: for small R procedure will converge, but there exists a critical value R_c beyond which the series diverges. Another way to see that these equations admit a critical behaviour, is to discretize momenta and treat (12) as the algebraic system of N ($N \rightarrow \infty$) polynomial equations. Again, for small R there exist a real solution which is just the recursive solution we displayed above. For $R > R_c$ this solution becomes complex indicating some singularity in the system. Needless to say that the critical values determined in both ways are consistent.

2.2. Singularities in the configuration space solutions

Existence of the two regimes in solutions of the configuration space equations (9) can be also readily established. Equation (9) is equivalent to the following system of two first order equations

$$\begin{aligned} \dot{\rho}(r) &= \sqrt{\sigma(r) - \frac{R_1(r)R_2(r)}{\rho}} \quad i.e. \quad \sigma \equiv \dot{\rho}^2 + \frac{R_1(r)R_2(r)}{\rho}, \\ \dot{\sigma}(r) &= \frac{1}{\rho(r)} \frac{d(R_1R_2)}{dr^2}. \end{aligned} \tag{14}$$

To satisfy boundary conditions (11) we solve (14) with

$$\rho(0) = 0, \quad \sigma(0) = \sigma_0, \tag{15}$$

and find a σ_0 such that $\sigma(\text{Max}(L_1, L_2)) = 1^2$. It turns out that real solutions satisfying this conditions exist only for $R < R_c$. This is illustrated in Fig. 1 where the solution $\sigma(1)$ is plotted as a function of the initial value σ_0 . Clearly our boundary conditions can be satisfied in this case. With increasing R the curve on Fig. 1 moves upwards and beyond some R_c real solutions cease to exist. Critical values determined from the configuration space solutions agree with those from the momentum space analysis. This is summarized in Table I where we compare R_c determined from the x - and p -analysis of three *gedanken* experiments:

- A. Head on collisions of the Lorentz-like sources with different shape parameters, d

$$s(r) = \frac{dL^4}{\pi(dL^4 + (1 - d)r^4)^{3/2}}, \quad d < L.$$

² For compact sources this is exactly equivalent to (11) because of the second equation (14). In practice the procedure also works for non-compact sources provided the distributions vanish quickly at large r . For example for identical Gaussian sources replacing $\text{Max}(L)$ with $10L$ is more than sufficient.

- B. Scattering of a central Gaussian source with a Gaussian ring for different widths of Gaussian distributions.
- C. Head on collision of two central Gaussian sources with different widths.

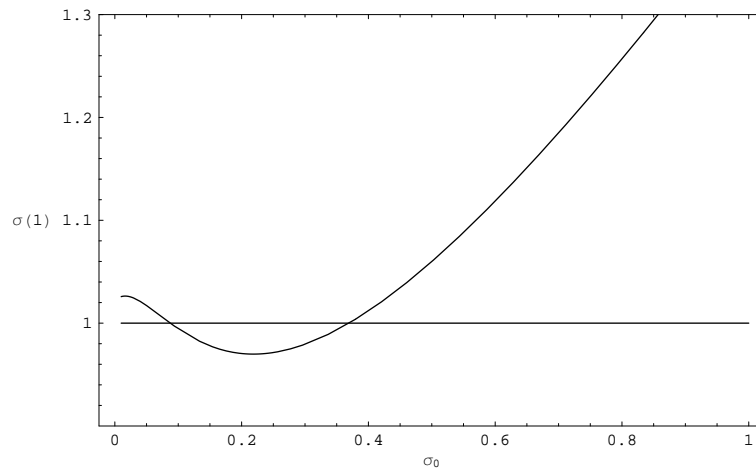


Fig. 1. Looking for the maximal solution of Eqs. (14), $\sigma(1) = 1$, as a function of the initial value $\sigma(0) = \sigma_0$ (in the specific case $d = 1$, $R/L = 0.46$).

In general both, x - and p -approaches give consistent results. For narrow sources (small σ or $d \ll 1, d \gg 1$) the momentum methods require yet finer discretization [16]. The case of the scattering of a point-like particle and a ring was solved analytically giving $R_c = 2^{1/2}/3^{3/4} \sim 0.62$ [13]. This is confirmed by our data B- x at $\sigma \rightarrow 0$ and equivalently A- x at $d \rightarrow \infty$.

3. Critical lines in the parameter space

Repeating above procedures for various parameters we have determined critical lines which separate dispersive and black hole (BH) phases in various parameter spaces [14]. Figure 2 shows such a line for the “experiment” C of Table I. The black hole phase is below the critical line corresponding to the high concentration of the incoming energy. Interestingly, the critical line is almost linear for a wide range of source sizes (right). This was also seen in Table I where the critical value of $R/(L_1 + L_2)$ was largely independent of the ratio $\rho = L_1/L_2$.

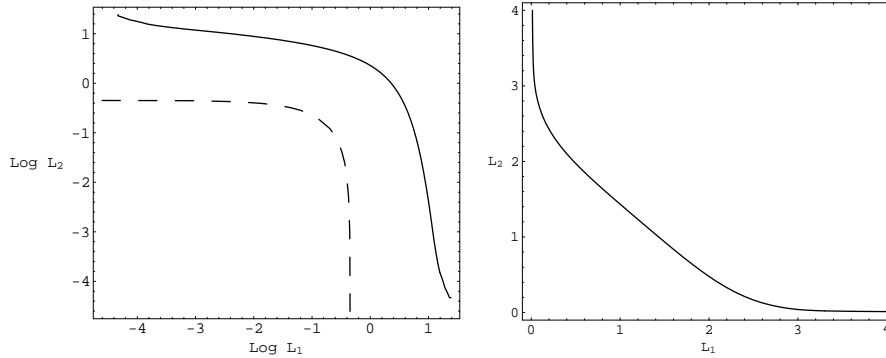


Fig. 2. A critical line (solid) in the (L_1, L_2) plane (case C of Table I). The lower bound (dashed) comes from the CTS criterion. A comparison between log–log (left) and the lin–lin (right) representations is also shown.

TABLE I

$(R/L)_c$ for a range of sizes of the power-like and Gaussian sources: a comparison between configuration and momentum-space results. A, B and C label sources as explained in the text. In the case C: $\rho = L_2/L_1$ and the critical value of the ratio $2R/(L_1 + L_2)$ is shown.

d	0.5	1.0	1.6	2.5	4.0		
A- x	0.419	0.471	0.502	0.528	0.550		
A- p	0.429	0.476	0.499	0.501	0.477		
σ	0.01	0.1	0.2	0.3	3.0		
B- x	0.615	0.572	0.525	0.486	0.470		
B- p	0.058	0.436	0.501	0.489	0.476		
ρ	0.25	0.333	0.5	1.0	2.0	3.0	4.0
C- x	0.810	0.816	0.821	0.823	0.821	0.816	0.810
C- p	0.823	0.833	0.850	0.841	0.838	0.840	0.832

3.1. Closed trapped surfaces

The dashed line in Fig. 2 (left) shows an estimate of the critical line given by the closed trapped surface (CTS) criterion. A CTS is a two-dimensional surface which is trapped below the horizon, that is both light rays emitted from different sides of the surface bend “downwards” ending on the singularity. It was shown by Kolparh and Veneziano that CTS exist if the source distribution satisfy a simple, symmetric self-consistency relation [17]

$$R_1(R_c)R_2(R_c) = R_c^2. \tag{16}$$

Existence of a CTS is a sufficient condition for a formation of a horizon and indeed the dashed line in Fig. 2 is located inside a BH phase. Interestingly, the CTS criterion reproduces reasonably well a shape of the transition line.

Figure 3 shows a similar phase diagram for the case A of Table I (head-on scattering of two Lorentzian sources). This time a BH phase lies above the the critical line and the upper bound, given by the CTS criterion, is again not far from the true transition.

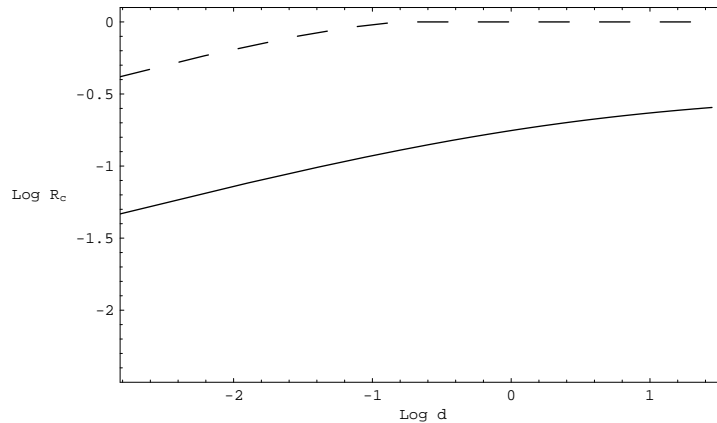


Fig. 3. The critical line (solid) in the (R, d) plane having set $L = 1$. We also show (dashed line) the upper bound on R_c from the CTS criterion (16). The BH phase is above the solid line.

4. On shell action and average multiplicity of gravitons

Criticality of the system shows up also in the action of our classical solutions. The action itself is infrared divergent, however its derivative with respect to some parameters is IR finite. In particular, the derivative over R^2 is IR finite. Incidentally it gives the average multiplicity of gravitons emitted in unit rapidity

$$\frac{\partial(\mathcal{A}/Gs)}{\partial R^2} = \frac{\pi^2}{R^3 \sqrt{s}} \langle N \rangle. \quad (17)$$

Consequently $\langle N \rangle$ does not have any IR divergence. At first sight this seems surprising since usually multiplicities of radiated quanta are not IR safe. It turns out however that in the axially symmetric case, considered here, only so called “TT” polarization is being produced and it is IR finite [13]. To see a typical bremsstrahlung like spectrum, one needs to access an “LT” mode of the gravitational field.

In Figure 4 we show the R dependence of Eq. (17) obtained from our numerical solution of (14). In the vicinity of the transition point the multiplicity is singular,

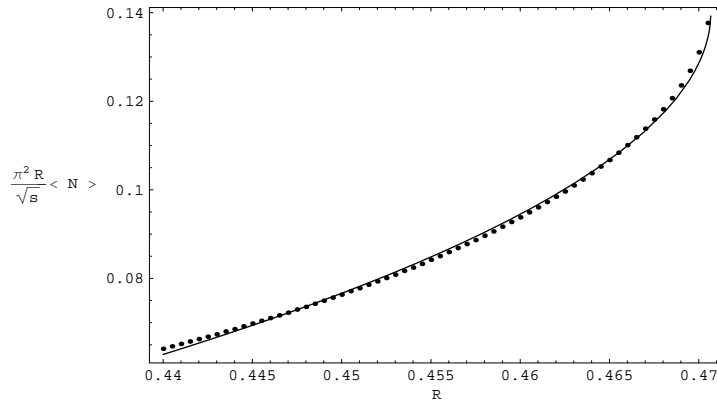


Fig. 4. The total multiplicity of emitted gravitons (points) and the best fit: $0.138 - 0.46(R_c - R)^{0.523}$. A fit with the fixed power $1/2$ is marginally worse.

with the singularity being consistent with a simple square root behaviour

$$\langle N \rangle = c_0 + c_1(R_c - R)^{1/2}. \tag{18}$$

This in turn means that the action of our classical solutions behaves as

$$A(R) = A_0 + A_1(R_c - R) + A_2(R_c - R)^{3/2}, \tag{19}$$

in agreement with findings of ACV [13].

It may be worth pointing out that, in statistical physics, half-integer values of critical exponents result usually from a mean field, or semi-classical, approximation. And indeed also in our case they follow from classical solutions of effective equations of motion.

As a second comment, notice that a range of R 's, or energies, covered in Fig. 4 is rather small. Consequently the rise of the multiplicity is quite spectacular when we approach the critical energy, even from the dispersive phase.

5. Spectra of gravitons

Having discussed total multiplicity we turn now to the differential distributions of emitted radiation [15]. In particular we would like to see if any singularity develops there while approaching the transition point, or if there are any properties of radiation carrying some information about the “other side” of the transition.

Figure 5 shows transverse momentum spectra of emitted gravitons for a range of R 's approaching a transition point. Two curves shown for each value of R give an idea of a dependence on the discretization parameter n^3 . Close to the criticality a sensitivity to the discretization is higher, the growth of the distribution itself also appears to be stronger. However there is no sign of any singularity, in k , developing at the critical point.

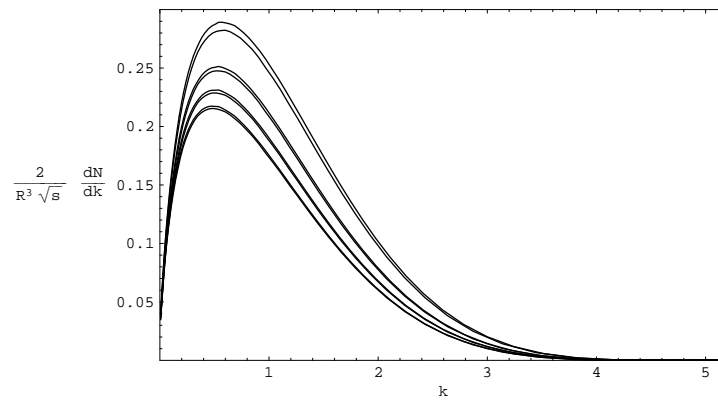


Fig. 5. Spectrum of gravitons (A). $R = 0.44, 0.45, 0.46, 0.47$; $R_c = 0.47067$, $n = 60-70$.

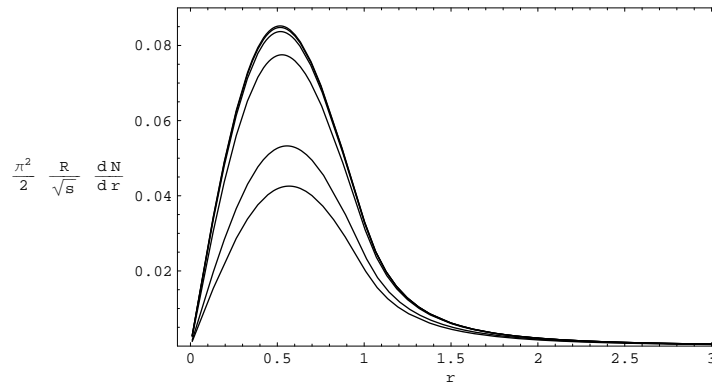


Fig. 6. Profile in the x -space, $R = 0.45, 0.46, 0.47, 0.4706, 0.47064, 0.47065$; $R_c = 0.470673$.

³ These results were obtained solving recursively the discretized set of equations (12).

The same conclusion follows from Fig. 6 where the transverse profile of the graviton field, in the configuration space, is shown. In both cases there exists a regular, limiting distribution of emitted gravitons when the transition point is approached from the dispersive phase. At the same time both, analytic (18) and numeric results, Figs. 4–6, show that it is approached with an infinite derivative.

It is perhaps interesting that the radiation is emitted preferentially from the distance $r \sim 0.5 * L$ from the source axes *cf.* Fig. 6⁴. Comparing with the critical value $R_c/L \cong 0.47$ we see that the maximum is close to the actual Schwarzschild radius of the horizon “just about to be formed” on the other side of the transition point.

Another such a “coincidence” can be extracted from Fig. 7 where the transverse spectra are shown on the logarithmic scale. Deep in the dispersive phase the distribution seems to have two components separated by a “knee”. Close to the transition, however, the knee vanishes leaving a single exponential at the transition point. Is this a tell-tale of the Hawking radiation present on the other side? If this is indeed so, than the slope of the exponential would be proportional to the mass of a black hole “to be formed”. Fig. 7 suggests that this slope does not vanish at criticality indicating that the transition considered here is of the first type.

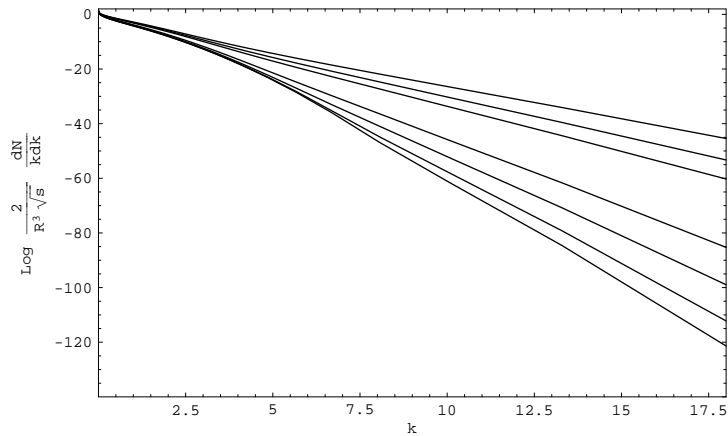


Fig. 7. Looking for the “Hawking temperature” of emitted gravitons. $R = 0.2, 0.3, 0.4, 0.6, 0.8, 0.82, 0.83; R_c = .841$.

⁴ We are talking here about the central collision of two sources of size L .

6. Complex trajectories

Obviously it is of great interest to examine our equations also in a BH phase. The simplest approach is to solve the large system of algebraic equations resulting from the discretization of equations (12) in the momentum space (*c.f.* Fig. 8). Below we discuss one exploratory example of such a procedure [15].

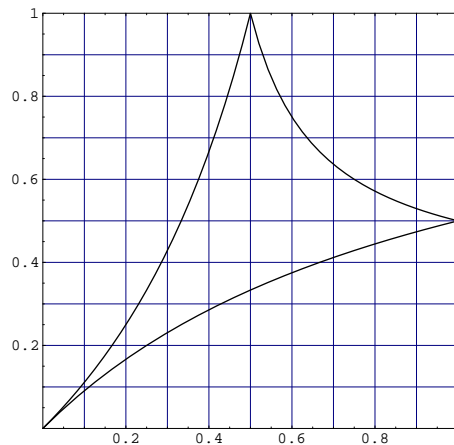


Fig. 8. The integration domain, in the compact v space, of the integral equations (12) and its discretization.

To reduce number of unknowns we eliminate $h(k)$ from the first equation and consider symmetric scattering with $s_1(k) = s_2(k)$. Upon dividing a compact range of a new variable $v = 1/(1 + kL)$ into n small intervals we are left with a system of n algebraic equations of third order. We then find all 3^n solutions with Mathematica and identify ones which are relevant in our case.

In Fig. 9 an example of two such solutions is shown. The figure displays a parametric plot of a value of $h(k)$ at one of the points, $k = k_3$, of a mesh. Points on a figure are labeled by R . Varying R one obtains a whole trajectory of $h(k_3)$ in a complex plane. In fact two, complex conjugate, trajectories are plotted. Let us trace them beginning deep in the dispersive phase.

For small $R < R_c$ trajectories are real. The left one coincides exactly with the recursive solution, which was independently generated. In fact we have checked, that this is the *only* (out of $3^6 = 726$) solution which is stable under the recursion. The second solution (beginning on the right of the pinch point) cannot be reached by the recursion. It is also real in the dispersive phase and it meets the recursive one at the critical point R_c . Points on both trajectories are initially separated by $\Delta R = 0.01$. When we approach R_c ,

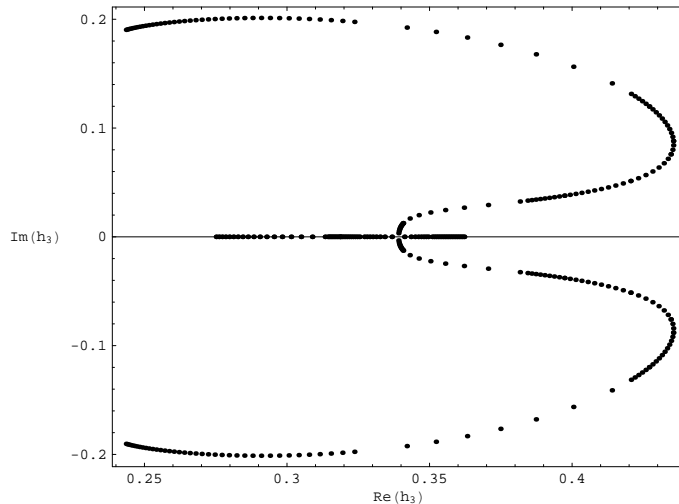


Fig. 9. Two complex trajectories of $h(k_3)$ parametrized by R moving across R_c .

$h(k_3)$ varies faster with R as expected and as is evident from the plot. Closer to R_c , ΔR was reduced to 0.001 to see this behaviour in more detail. After passing R_c both trajectories acquire imaginary, complex conjugated, parts with a typical threshold behaviour. We have found a rich structure deeper in the BH phase, for example there are other trajectories which seem to cross the two shown here. Since however the interpretation of complex solution is far from complete, we refrain from pushing the subject any further.

One thing, however, is clear: complex solutions of classical equations of motion, imply complex action which indicates existence of some instabilities in the system. The whole phenomenon is reminiscent of the discussion of a “fate of a false vacuum” by Coleman with complex saddle points playing analogous roles [18]. There is also an interesting recent attempt to understand these solutions in somewhat simpler quantum mechanical model [19].

7. Summary

The effective action of Amati, Ciafaloni and Veneziano allows for quantitative study of a scattering of gravitating sources in the transplanckian, $Gs \gg 1$ regime. Interestingly, summing eikonal diagrams together with the single emissions in the s -channel is sufficient to produce some signatures characteristic of a gravitational collapse.

Recent solutions of the effective equations of motion reveal existence of the two phases corresponding to the dispersive and collapsing behaviour. In this paper we have discussed how the onset of the transition between the

two regimes occurs and studied in detail singularity of the on mass shell action and production of gravitons in the dispersive phase but close to the criticality.

Our numerical calculations confirm that the OEM action scales in the vicinity of a transition point with the mean field (or classical) value of the exponent obtained analytically by ACV. That value is numerically close to twice of the one obtained by Choptuik in his solutions of the full Einstein equations.

The limiting distribution of the radiation, approached from the dispersive phase, is regular. It is peaked around the horizon, (to be formed at the other side of a transition) and displays a simple exponential dependence on a graviton transverse momentum. The slope of that exponential does not vanish at the critical point, suggesting that the transition may be of the first type.

Finally, the solutions become complex in the black hole phase signaling instabilities in the system and/or possible opening of new channels.

All results reviewed here have been obtained in collaboration with Gabriele Veneziano. I thank him for numerous and stimulating discussions on many issues. This work was completed while visiting the Theory Group in the Max-Planck Institute (W. Heisenberg Institute) in Munich. I thank them for their hospitality.

REFERENCES

- [1] M.W. Choptuik, *Phys. Rev. Lett.* **70**, 9 (1993).
- [2] P. Breitenlohner, P. Forgacs, D. Maison, *Comm. Math. Phys.* **261**, 569 (2006).
- [3] P. Bizon, T. Chmaj, B.G. Schmidt, *Phys. Rev. Lett.* **97**, 131101 (2006).
- [4] C. Gundlach, J.M. Martin-Garcia, *Living Rev. Rel.* **10**, 5 (2007) [0711.4620 [gr-qc]].
- [5] J. Sherk, J.H. Schwarz, *Gen. Rel. Grav.* **6**, 537 (1975).
- [6] M. Kaku, *Nucl. Phys.* **B91**, 91 (1975).
- [7] C. Aragone, J. Chela-Flores, *Nuovo Cim.* **B25**, 225 (1975).
- [8] D. Amati, M. Ciafaloni, G. Veneziano, *Phys. Lett.* **B197**, 81 (1987); *Int. J. Mod. Phys.* **A3**, 1615 (1988).
- [9] L.N. Lipatov, *Phys. Lett.* **B116**, 171 (1982); *Nucl. Phys.* **B365**, 614 (1991).
- [10] L.N. Lipatov, *Nucl. Phys.* **B307**, 705 (1988).
- [11] D. Amati, M. Ciafaloni, G. Veneziano, *Nucl. Phys.* **B403**, 707 (1993); *Nucl. Phys.* **B347**, 550 (1990).

- [12] R. Kirschner, L. Szymanowski, *Phys. Rev.* **D52**, 2333 (1995).
- [13] D. Amati, M. Ciafaloni, G. Veneziano, *J. High Energy Phys.* **02**, 049 (2008).
- [14] G. Veneziano, J. Wosiek, *J. High Energy Phys.* **09**, 023 (2008).
- [15] G. Veneziano, J. Wosiek, *J. High Energy Phys.* **09**, 024 (2008).
- [16] G. Marchesini, E. Onofri, *J. High Energy Phys.* **06**, 104 (2008).
- [17] E. Kohlprath, G. Veneziano, *J. High Energy Phys.* **06**, 057 (2002).
- [18] S. Coleman, F. de Luccia, *Phys. Rev.* **D21**, 3305 (1980).
- [19] M. Ciafaloni, D. Colferai, [0807.2117 [hep-th]].